Molten chloride salts for next generation CSP plants: Electrolytical salt purification for reducing corrosive impurity

Wenjin Ding[a,*], Judith Gomez-Vidal[b], Alexander Bonk[a], Thomas Bauer[c]

[a]*Institute of Engineering Thermodynamics, German Aerospace Center (DLR), Stuttgart, Germany*

[b]*Building and Thermal Sciences Center, National Renewable Energy Laboratory (NREL), Golden, Colorado, USA*

[c]*Institute of Engineering Thermodynamics, German Aerospace Center (DLR), Cologne, Germany*

*Corresponding author. Tel.: +49 2203 601 3162. E-mail address: wenjin.ding@dlr.de.

Abstract

In this work, electrolysis with a Mg anode is presented to purify the molten chloride salt ($MgCl_2$/KCl/NaCl 60/20/20 mol.%) for reducing its corrosivity. Using a Mg anode, the production of toxic gases like Cl_2 on an inert anode (e.g., tungsten) can be avoided. Moreover, compared to an inert anode, a lower over-potential is required to remove corrosive impurity $MgOH^+$ in the molten salt due to high reactivity of Mg. In order to evaluate the effect of the salt purification, the cyclic voltammetry (CV) method developed in our previous work is used to in-situ measure the concentration of the corrosive impurity in the molten salt. The CV measurements indicate that the corrosive impurity is efficiently removed by electrolysis. The potentiodynamic polarization (PDP) measurements on a commercial high-temperature alloy (Incoloy 800 H) immersed in the molten salt indicate that the corrosion rate of the alloy is significantly reduced due to the salt purification. For decreasing the cathode inactivation due to produced MgO on the surface, a pulsed potential applied on the tungsten cathode during electrolysis shows to be promising. This electrochemical salt purification method has shown to be promising by efficiently controlling the corrosivity of the molten chloride salt. It could also lead to a reduction of the cost of the salt purification, structural container materials, and piping in next generation concentrated solar power (Gen3 CSP) plants.

Graphical abstract

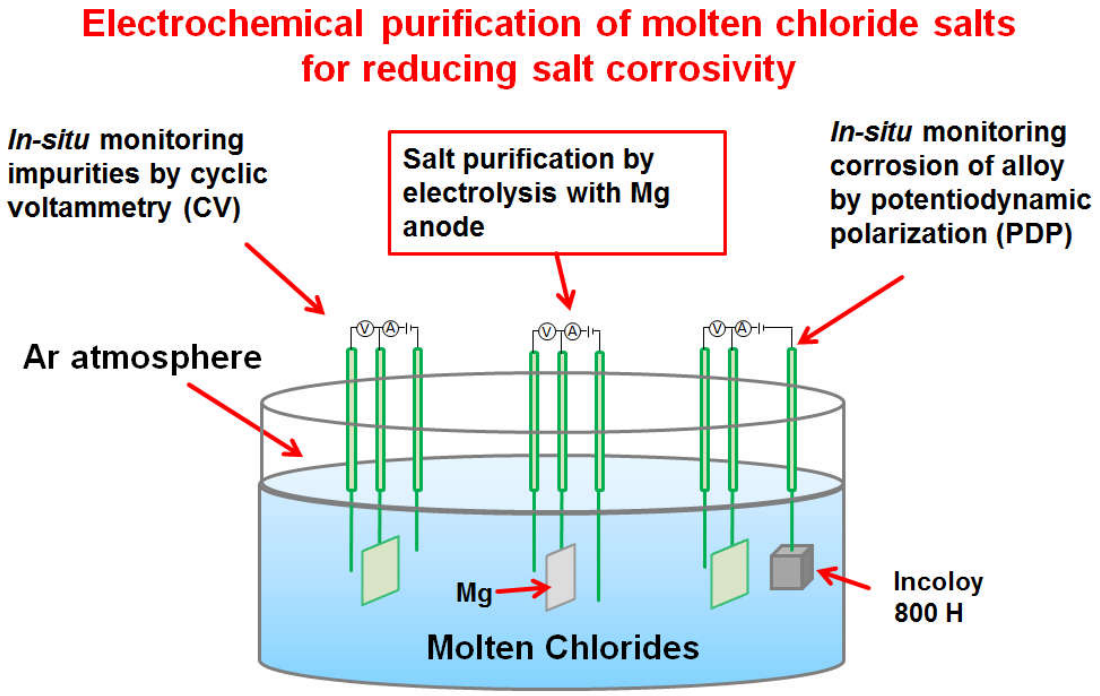

Highlights

- Electrolysis with a Mg anode purifies a molten chloride salt to reduce its corrosivity.
- Cathode passivation due to produced MgO at the surface is significantly reduced by applying pulsed potential.
- Cyclic voltammetry shows that concentration of corrosive impurity in purified salt is reduced to ~7% compared to the unpurified salt.
- Potentiodynamic polarization of Incoloy 800 H in purified salt indicates ~80% corrosion rate reduction compared to that in unpurified salt.

Keywords

Concentrated solar power (CSP); Corrosion control; Corrosive impurity; Cyclic voltammetry (CV); Electrolysis; Potentiodynamic polarization (PDP).

1. Introduction

Concentrated solar power (CSP) technology is emerging as one of the important technologies in the future renewable energy system [1]. CSP plants concentrate a large area of sunlight onto a small area (receiver) by using mirrors or lenses to generate solar power. Electricity is generated when the concentrated light is converted to heat, which drives a heat engine connected to an electrical power generator. In commercial CSP plants, heat storage (thermal energy storage) in molten salts, e.g., nitrate salt mixtures, allows CSP plants to generate dispatchable power during the absence of sunlight and adds value to such power plants when compared to photovoltaic panels.

Molten chloride salt mixtures such as $MgCl_2$/KCl/NaCl (melting temperature: ~380°C) are promising thermal energy storage (TES) materials to store the heat from sunlight in next generation CSP plants [2], due to their high thermal stability (stable at >800°C [3-4]), good thermal conductivity, good heat capacity but low prices [3-8]. In particular, their high thermal stability makes them appropriate candidates to replace the commercial nitrate salt mixtures, which are decomposed at ~550°C [9-11], when higher operating temperatures (e.g. 700°C) are required for higher efficiency of thermal to electrical energy conversion in next generation CSP plants [2].

However, the application of molten chloride salts at high temperatures causes additional challenges, particularly increased corrosiveness of containers and structural materials [12-18]. It is well known that corrosion rates significantly depend on the concentration of hydroxide/O_2 impurities in the molten chloride salts [12,16-18]. The corrosive impurities come mainly from water- and O_2-dissolved compounds in the chloride salts, as well as from the presence of moisture and O_2 in the atmosphere [12,16-22]. The introduction of hydrated compounds in the chloride salts (e.g., $MgCl_2$, a strong hygroscopic chloride salt) - induces its hydrolysis during heating following the simplified Eqs. (1-2) to produce corrosive HCl and MgOHCl [19,22]. These molecules react with the containers and structural materials (i.e., alloys) according to the simplified Eqs. (3-4). Oxygen containing species existing in the chloride salts (e.g. dissolved O_2) and in the atmosphere, corrode the containers and structural materials by oxidizing the alloying components as shown in the simplified Eq. (5) [22]. More details about the corrosion behaviors and mechanisms of Cr-Fe-Ni alloys in molten chloride salts can be found in the open literature [15,22-23]. Reviews on hot corrosion of metallic alloys in molten salts [16] and corrosion control in chloride and fluoride salts [8,17] are suggested.

$$MgCl_2 + H_2O \rightarrow MgO + 2\,HCl, \qquad \text{Eq. (1)}$$

$$MgCl_2 + H_2O \rightarrow MgOHCl + HCl, \quad \text{Eq. (2)}$$

$$x\ HCl + M \rightarrow MCl_x + (x/2)\ H_2, \quad \text{Eq. (3)}$$

$$x\ MgOHCl + M \rightarrow x\ MgO + MCl_x + (x/2)\ H_2, \quad \text{Eq. (4)}$$

$$x/2\ O_2 + y\ M \rightarrow M_yO_x, \quad \text{Eq. (5)}$$

M = the alloying element in the alloy, e.g., Cr in Cr-Fe-Ni alloys. The thermodynamic calculations using the commercial software – FactSage® show that the standard Gibbs free energy of the reaction between MgOHCl and the alloying element Cr, Fe and Ni at 700°C is -100, -50.7 and -17.1 kJ/mol, respectively.

In order to realize the commercial application of molten chloride salts at high temperatures, some techniques [21,24-30] used to reduce the corrosivity of the molten chloride salts have been investigated. Examples of them are: i) by a chlorinating process (CCl_4, HCl, or other chlorinating compounds [21,24-25]) to reduce the hydrolysis reaction, ii) by adding active metals such as Mg and Li [26-30] in the salt, in order to reduce the redox potential of the melt. Using active metals (e.g., Mg), the corrosive impurities preferentially react with them instead of oxidizing the alloying elements:

$$2\ MgOHCl + Mg \rightarrow MgCl_2 + 2\ MgO(s) + ½\ H_2\ (g), \quad \text{Eq. (6)}$$

$$O_2 + 2\ Mg \rightarrow 2\ MgO(s). \quad \text{Eq. (7)}$$

The results of adding 1.15 mol.% Mg in $MgCl_2$-KCl [27] showed that the corrosion rate (CR) of the Ni-based Cr-Fe-Ni alloy (Hastelloy 230) under inert atmosphere at 850°C reported 35 times lower corrosion than baseline tests without Mg, and its reduced CR met the alloy requirements for industrial applications (CR < 15 μm/year). Additional aggravated corrosion experiments, by using convective-flow thermosiphon, showed that the CR in convective flow with no Mg additive increased by a factor of three [27], whereas thermosiphon tests with 1.15 mol.% Mg showed the CR below 15 μm/year [27]. However, this corrosion mitigation method was not studied in real solar power applications, and the corrosion mitigation mechanism was not investigated in detail [27]. In our previous work [31], three commercial high temperature Fe-Cr-Ni alloys (SS 310, Incoloy 800 H and Hastelloy C-276) were exposed to molten $MgCl_2$-NaCl-KCl (60–20–20 mol%) mixed salts with 1 wt.% Mg as corrosion inhibitor, for 500 h at 700 °C under inert atmosphere. The corrosion mitigation mechanism of Fe-Cr-Ni based alloys in molten chloride salts by adding Mg was discussed based on corrosion thermodynamics and microstructural analysis on the corroded alloy samples [31].

To in-depth investigate corrosion behavior and mechanism of alloys in molten chloride salts, some electrochemical methods have been studied or used in corrosion tests, and have shown to be useful tools [32-35]. For instance, our previous work [32-33] and the open literature [36] show that an electrochemical method based on cyclic voltammetry (CV) could

reliably, fast but affordably, measure the concentrations of corrosive impurities in molten chloride salts. It provides unique possibility to in-situ monitor impurity concentrations and thus assists the technological processes for corrosion control [32-33,36]. Another electrochemical method, based on potentiodynamic polarization (PDP), has been often used to in-situ and fast-measure the corrosion potential and CR of an alloy in molten salts [34-35]. By analyzing these tested values, the corrosion behavior and mechanism of studied alloys in molten chloride salts were better understood [34-35].

In this work, a purification method based on electrolysis of impurities in molten chloride salts is investigated. A Mg-anode is used in this method to reduce the corrosive impurities in the molten chloride salts mainly hydroxide species (DLR and NREL jointly filed U.S. Patent Application 16/003,229 [37]). To our best knowledge, such work is not available in open literature. In order to evaluate the salt purification effectiveness, CV is used to determine the impurity concentration of the molten chloride salt. In addition, PDP method is used to measure the corrosivity of the purified and unpurified salts by measuring the corrosion rate of a common commercial high-temperature alloy (Incoloy 800 H) in the molten chloride salt. The salt mixture of $MgCl_2$/KCl/NaCl (60/20/20 mol.%) was used for the experiments.

2. Experimental

2.1. Experimental set-up

Figure 1 shows a schematic of the experimental set-up used for the salt electrochemical purification, CV and PDP experiments. A high temperature resistance glassy carbon crucible purchased from *HTW* Germany (Sigradur® G) was used to avoid the reaction of the molten chloride salt with the crucible material. During the experiments (procedures will be described in section 2.2), the temperature of the molten salt in an argon atmosphere was controlled by the programmable furnace and the thermocouple located close to the molten salt surface (see Figure 1). For CV and PDP experiments, an Al_2O_3 plate was used under the glassy carbon crucible to isolate it from other metallic parts of the experimental set-up.

As shown in Figure 1, six electrodes were used for the electrochemical purification, CV and PDP experiments. A tungsten electrode immersed in the molten salt was used as the quasi-reference electrode for all the electrochemical experiments. All the electrochemical experiments were conducted using a ZENNIUM electrochemical workstation from *Zahner GmbH* (Germany). Table 1 shows which electrodes were used in each type of experiment and which materials were used for those electrodes. The Mg electrode (electrode Nr. 6) was used as the anode for the salt electrochemical purification. The pure tungsten wire used in

this work, for the electrodes or electrode parts, was purchased from *Alfa Aesar* (purity ≥ 99.95 %, diameter: 1 mm). In the CV experiments, the immersion depth of the working tungsten electrode was fixed to 5 mm by using an ohmmeter (i.e., the contact area of the tungsten electrode with the melt is 16.5 mm^2), while the counter and reference electrodes had a much larger immersed area, as shown in Figure 1. More details about CV experiments can be found in our previous work [32-33] and section 2.3.2.

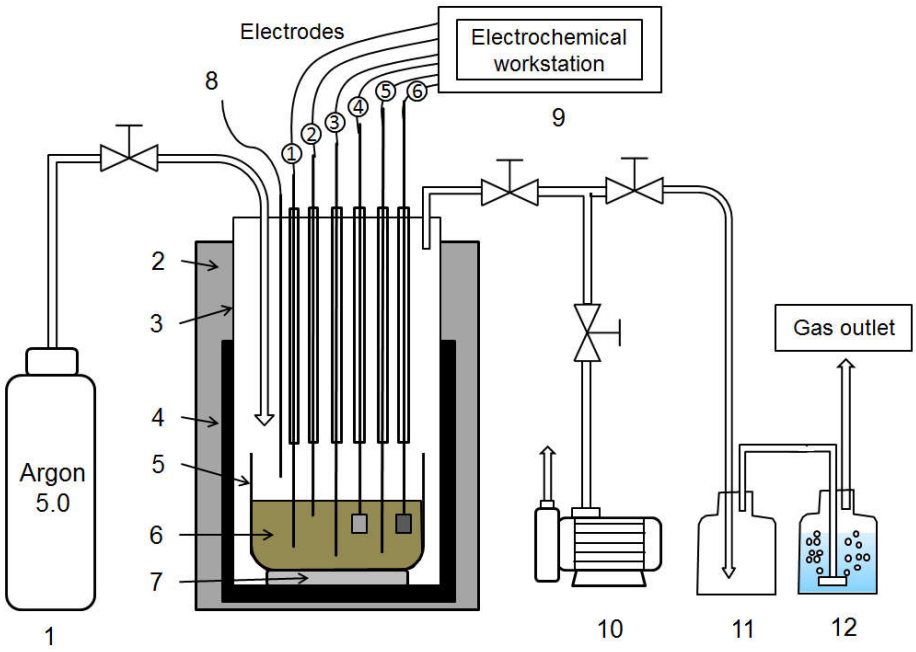

Figure 1: Schematic of experimental set-up for electrochemical salt purification using a Mg anode, CV and PDP experiments. 1: Storage tank for argon 5.0 gas, 2: Glass wool heat isolator, 3: Steeling tube of Incoloy 800 H, 4: Furnace, 5: Glassy carbon crucible, 6: Molten chloride salt, 7: Al_2O_3 plate, 8: Thermocouple close to the molten salt, 9: Electrochemical workstation for electrochemical experiments, 10: Vacuum pump, 11: Security bottle (empty) for reflux from the bottle for gas washing, 12: Bottle with NaOH solution for gas washing (removal of HCl and Cl_2).

Table 1: Electrodes used for electrochemical purification, measuring the impurity concentration via CV as well as monitoring corrosion potential and corrosion rate of studied alloy via PDP.

Experiments	Applications	Electrode identified in Figure 1		
		Working	Counter	Reference
Electrolysis	Electrochemical purification	6	5	1
CV	Measuring impurity concentration	2	3	1
PDP	Corrosion potential / rate of studied alloy	4	3	1

1: Tungsten quasi-reference electrode, 2: Tungsten working electrode,

3: Tungsten counter electrode, 4: Alloy sample (Incoloy 800 H) + tungsten wire,

5: Tungsten cathode for salt purification,

6: Mg anode (~0.5 g, purity ≥ 99.5%, *Sigma Aldrich*, Germany) + tungsten wire for salt purification.

2.2. Procedures

KCl(99%) and NaCl(99%) were purchased from *Alfa Aesar*, Germany, while anhydrous $MgCl_2$(99%) came from *Magnesia*, Germany. The anhydrous $MgCl_2$ was expected to have small amounts of hydrated $MgCl_2$ due to the short-time in contact with room air. They were used to synthesize the salt mixture of $MgCl_2$/KCl/NaCl (60/20/20 mol.%, melting temperature ~400°C) for the experiments. Referring to our previous work [20,22], the heating process of the salts is performed as follow: after vacuuming by the vacuum pump for 30 minutes (≤ 30 mbar), the salt mixture (~140 g) was heated (heating rate of ~5°C/min) under an argon atmosphere (Argon 5.0, purity ≥ 99.999%, H_2O ≤ 3 ppm, O_2 ≤ 2 ppm, 30 nL/h, pressure above atmospheric pressure is about 0.1 bar) to 200°C, then kept at 200°C for 1 hour to release the hydrated water and to reduce the side reaction to hydroxides and HCl (Eqs. 1-2).

In **Experiment 1**, the salt was heated to 500°C (heating rate of ~5°C/min) **in the first stage**. The concentration of the corrosive impurity $MgOH^+$ before the salt purification was measured with the CV method. Then, the molten salt was purified by electrolysis with the Mg anode, which will be introduced in Section 2.3.1 in detail. After the electrochemical purification, the used Mg anode was removed from the molten salt, but kept in the cold part of the autoclave, where the temperature during the experiment was below the melting temperature of Mg. The concentration of the corrosive impurity was measured again with the CV method to determine the salt purification level. **In the second stage**, the molten salt was heated to 700°C (the expected operating temperature of molten chlorides in CSP) with the heating rate of ~5°C/min to study its corrosivity. When the salt had a temperature of 700°C, a common commercial high-temperature alloy (Incoloy 800 H, size: ~10×10×15 mm), i.e., electrode Nr. 4 in Table 1, was immersed in the purified molten salt. Its corrosion rate and corrosion potential were measured by the PDP method. The composition of Incoloy 800 H is shown in Table 2. The Mg anode used in the first stage was immersed again into the molten salt. Because elemental Mg has a melting point of ~650°C, it melted and gradually dissolved into the molten salt to keep a low corrosivity (solubility of Mg in $MgCl_2$/KCl 50/50 mol.% and $MgCl_2$/NaCl 50/50 mol.% at 700°C: 0.2-0.3 mol.% [38]). At 700°C, the corrosivity of the molten salt was studied for over 450 h via determining the corrosion potential and CR of Incoloy 800 H using the PDP method, while the CV method was used to monitor the salt chemistry of the molten salt.

In the comparative experiment (**Experiment 2**), the salt mixture with the same composition as that used in Experiment 1 was directly heated from 200°C to 700°C without any electrochemical purification with the heating rate of ~5°C/min. The corrosivity of the

unpurified molten salt was also studied at 700°C by using the same Incoloy 800 H electrode for 340 h via CV and PDP.

Table 2: Composition of Incoloy 800 H (In 800 H) measured by the supplier (main elements) (wt.%).

Alloy	Fe	Ni	Cr	Mn	Si
In 800 H	Balance	29.40	20.84	1.06	0.78

2.3. Methods

2.3.1. Salt purification by electrolysis with Mg anode

In the salt electrochemical purification at 500°C, an over-potential (vs. the reference potential of W quasi-reference electrode) was applied on the anode and cathode immersed in the molten salt. The level of applied voltage (over-potential) depends on the electrode materials and the impurity to be removed. According to the cyclic voltammogram at 500°C as shown in Figure 2, a potential of -1.25 V vs. the reference potential (between peak A and B) was applied on the W cathode in this work. Therefore, the following reactions take place at the cathode and anode during the electrochemical salt purification, respectively:

Cathode (Reduction): $2MgOH^+ + 2e^- = 2MgO(s) + H_2(g)$ (I)

Anode (Oxidation): $Mg(s) = Mg^{2+} + 2e^-$ (II)

Total Reaction: $2MgOH^+ + Mg(s) = Mg^{2+} + 2MgO(s) + H_2(g)$ (III)

Reaction (I) shows that the corrosive species $MgOH^+$ is reduced at the cathode, to form MgO and H_2. As MgO is hardly soluble in the molten chloride salts [32], it either remains at the cathode or precipitates in the molten salt. Because MgO is none electrically conductive, remaining at the cathode can decrease the active area of the electrode and thus lead to cathode passivation, and reduced electrolysis efficiency. At the Mg anode, Mg^{2+} is formed. In total, the Mg anode is consumed, while at the cathode the impurity $MgOH^+$ reacts to insoluble MgO and other products, e.g., H_2, which can escape.

2.3.2. Cyclic voltammetry for measuring concentration of impurity

Figure 2 shows a representative cyclic voltammogram from our previous work for unpurified $MgCl_2$/KCl/NaCl (60/20/20 mol.%) with the impurity $MgOH^+$ determined at 500°C [32]. The peaks A, A', B and C in Figure 2 represent the following electrochemical reactions, respectively:

Reaction A: $Mg^{2+} + 2e^- = Mg$ Eq. (8)

Reaction A': $Mg = Mg^{2+} + 2e^-$ Eq. (9)

Reaction B: $MgOH^+ + e^- = MgO + ½ H_2$ Eq. (10)

Reaction C: $Cl^- = ½ Cl_2 + e^-$ Eq. (11)

Our previous work [32-33] and the literature [36] show that the bulk concentration of the corrosive impurity $MgOH^+$ in the molten $MgCl_2$/KCl/NaCl salt is proportional to the peak current density of the peak B, $i_p(B)$ in mA/cm^2 at 500-700°C as follows:

$$c^{\infty}(MgOH^+) = k(T,\nu)\cdot i_p(B)\,, \qquad \text{Eq. (12)}$$

where $i_p(B)$ represents the peak current density of peak B in mA/cm^2 (see Figure 2); $k(T,\nu)$ is a constant, i.e., slope of peak current densities vs. concentrations of the reacting species $MgOH^+$ in (ppm Oxygen in weight)/(mA/cm^2), which depends on the temperature T and ν potential sweep rate; c^{∞} is the bulk concentrations of the reacting species $MgOH^+$ in ppm O in weight. Under the potential sweep rate of 200 mV/s in CV, $k(T,\nu)$ is **38.2±7.6** and **9.4±1.9** (ppm O)/(mA/cm^2) for $MgOH^+$ in the studied molten $MgCl_2$/KCl/NaCl salt at 500 and 700°C, respectively [33]. In this work, the peak current density of peak B obtained from CV and the k constants identified in previous work [33] from CV and titration were used to calculate the concentration of the impurity $MgOH^+$ in the molten salt.

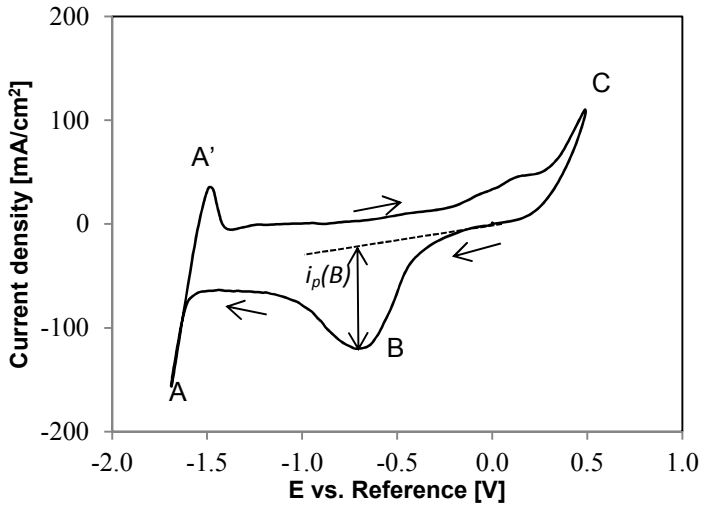

Figure 2: Cyclic voltammogram obtained on a tungsten working electrode in $MgCl_2$/KCl/NaCl (60/20/20 mol%) at 500 °C adopted from [32]. Sweep rate: 200 mV/s. $i_p(B)$: peak current density for reaction B. A tungsten counter and quasi-reference electrode were used.

2.3.3. Potentiodynamic polarization for estimating salt corrosivity

PDP method was used to estimate the corrosion rate of the studied alloy (Incoloy 800 H) immersed in the molten salt. Before the potentiodynamic polarization sweep tests, the alloy

and other electrodes were immersed in the molten salt for ~30 min, so that the stable open circuit potential (OCP) of the alloy was established, i.e., the OCP reached quasi-equilibrium (d(OCP)/dt ≤ 1 mV/s) [34]. The PDP tests were performed by applying cathodic (-) and anodic (+) external potentials, sweeping from -60 mV to +60 mV relative to the OCP value at 1 mV/s [6,34]. Every PDP test was repeated to evaluate the reproducibility of the results. After the PDP tests, the corrosion current obtained with PDP was used to calculate an estimated corrosion rate according to Faraday law [34-35]:

$$CR = k[\frac{I_{corr} \cdot EW}{\rho \cdot A}], \quad \text{Eq. (13)}$$

where the corrosion rate (CR) has the unit of μm per year, k = 3.27 in μm g μA^{-1} cm^{-1} yr^{-1}; I_{corr} is the corrosion current obtained from Tafel slopes (as shown in Figure 8) in μA; A is the contact area of the working electrode (studied alloys) with molten chlorides (~7.6 cm^2), in this work changes of the surface area due to repetitive PDP tests were neglected; *EW* and *ρ* are equivalent weight (dimensionless, 25.04 for Incoloy 800 H) and density in g cm^{-3} (7.94 g cm^{-3} for Incoloy 800 H) of the alloy sample, respectively [34-35].

2.3.4. Atomic absorption spectroscopy (AAS) for salt post-analysis

The concentrations of Cr, Fe and Ni in the salt samples after Experiments 1 and 2 (see Section 2.2) were measured with an atomic absorption spectrometer (iCE 3000 series, *Thermo Scientific*, US) with deuterium background correction. A hollow cathode lamp was used as the radiation source with a current of 12 mA for Cr and 10 mA for Fe/Ni. The main analytical lines at 357.9 nm, 248.3 nm and 232.0 nm with a spectral bandwidth of 0.2-0.5 nm were used for Cr, Fe and Ni, respectively. The spectrometer data was analyzed with the operational software Solaar AA Version 11.03. Integrated absorbance (peak area) was used exclusively for signal evaluation and quantification. In the calibration measurements, three standard solutions with the concentrations of 1, 2 and 5 mg/L for each element were prepared by dissolving the corresponding chloride salt in 100 mL demineralized water + 1 mL 1wt.% HCl + 10 mL 10wt.% CsCl solution. In the AAS measurements, ~100 mg salt sample was dissolved in the 100 mL VE water + 1 mL 1wt.% HCl + 10 mL 10wt.% CsCl solution and then its concentration was measured. Note that, the salt sample from the center part of the salt block after Experiments 1 and 2 was used, in order to avoid some undissolved precipitates in the solution. For the theory about AAS and how to use AAS, the book of B. Welz and M. Sperling [39] is suggested.

The concentrations of alloying elements dissolved in the chloride salt can be used to estimate the equivalent corrosion depths (ECD) of the alloys with the following equation:

$$ECD = \frac{M_{salt} \cdot \left(\sum_{i=1}^{n} \frac{x_i}{\rho_i}\right)}{A \cdot t} \cdot 10^4 \cdot 24 \cdot 365, \quad \text{Eq. (14)}$$

where the ECD has the unit of μm per year; M_{salt} is the weight of the molten salt used in this study in g (~140 g); *x* and *ρ* are the mass fraction of the alloy elements dissolved in the melt and density of the alloy elements in g cm^{-3} (7.19 g cm^{-3} for Cr and 7.87 g cm^{-3} for Fe), respectively; *t* is the experiment time in h (Experiment 1: 450 h; Experiment 2: 340 h). Note that, the ECD estimated with this method is underestimated compared to the CR determined with the conventional methods [22] or electrochemical methods like PDP, due to the corrosion products (i.e., Cr and Fe oxides) remaining at the alloy surface and precipitating in the melt.

3. Results and discussion

3.1. Electrochemical salt purification

In **Experiment 1**, once the salt was heated to 500°C and before electrochemical purification, a significant peak representing the reduction of $MgOH^+$ to MgO and H_2 (peak B) was observed in the cyclic voltammogram (Figure 3). The peak current of peak B was ~70 mA, i.e., the peak current density was ~438 mA/cm^2, as the contact area of the working electrode with the melt was ~0.16 cm^2. This means that the concentration of $MgOH^+$ in the melt was ~16713±3325 ppm O in weight according to Eq. (12).

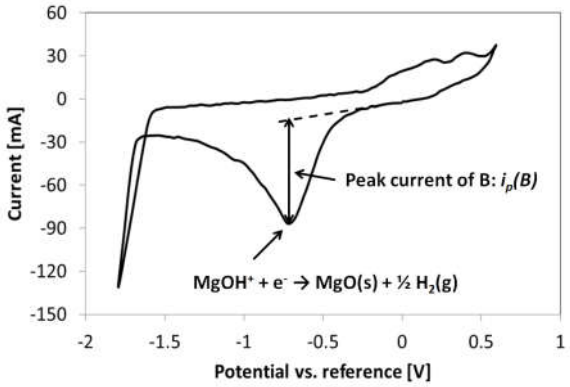

Figure 3: Cyclic voltammograms of molten $MgCl_2$/NaCl/KCl (60-20-20 mol%) at 500°C before electrochemical salt purification. Sweep rate: 200 mV/s. $i_p(B)$: peak current for reaction B.

Before purification, the electrodes were immersed in the melt for ~30 min to activate the surfaces, particularly for the Mg anode. A potential of -1.25 V vs. the reference potential was applied on the W cathode in the electrochemical purification at 500°C. The results showed that after only ~3 min, the electrolysis current was reduced to <30% of the start value due to

the cathode passivation (see Figure 4). Moreover, CV showed that the peak B did no significantly change (the peak height had a decrease of ~15%), even after 60 min of electrolysis. It was observed after the electrolysis that a lump deposited on the surface of the tungsten cathode, as shown in Figure 5 b). According to reaction (I) in section 2.3.2, MgO was assumed to be produced at the cathode due to the electrolysis. As shown in Figure 6, the energy-dispersive X-ray spectroscopy (EDS) measurement on the lump confirmed that it consisted mainly of Mg (>55 wt.%) and O (>37 wt.%).

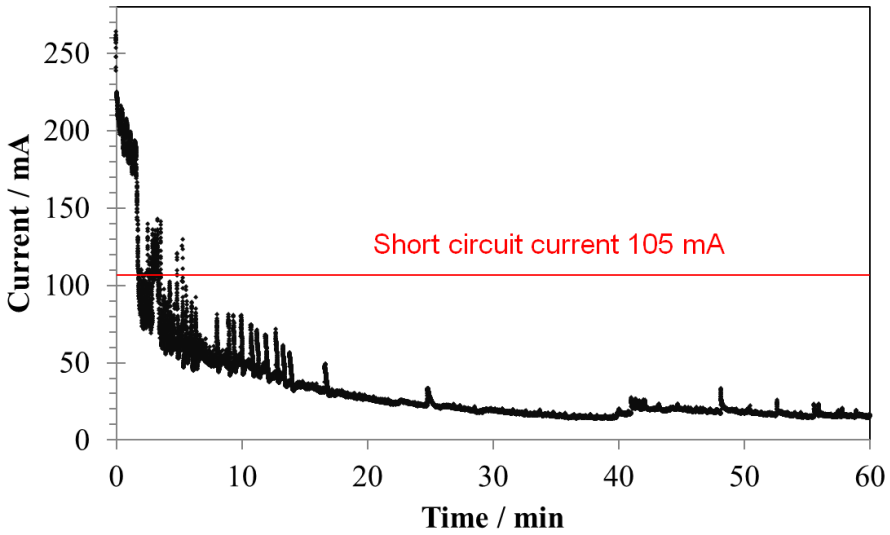

Figure 4: Change of electrolysis current with the time in electrolysis with a Mg-anode, W-cathode and W-reference electrode. A potential of -1.25 V vs. the reference potential was applied on the W cathode. The short circuit current was ~105 mA when the fresh Mg-anode and W-cathode were connected but no over voltage was applied on them.

The deposition of MgO on the cathode leaded to the passivation of this electrode, causing a significant reduction of the electrolysis current. In this work, by applying a pulsed potential on the cathode as shown in Figure 7a), it was found that the passivation of the cathode due to produced MgO could be significantly reduced. There was an interval of 1.5 min between 0.5 min electrochemical salt purification steps. Larger currents could be regained when the applied voltage was stopped (i.e. 0 V) for a 1.5 min duration after each electrolysis. It was assumed that this effect might be due to peeling-off of the thin MgO layer from the cathodic surface in the interval when the electrolysis stopped (schematically shown in Figure 8). The duration of the electrochemical purification was determined by a current measurement over time, while the interval time between the electrolysis was measured by the experiments. In this work, when the current had a ~10% drop compared to the initial value after ~0.5 min salt purification (see Figure 4), the applied voltage was stopped for 1.5 min as shown in Figure 7a). In our future work, the duration of the electrochemical purification and interval time can be optimized according to the application conditions.

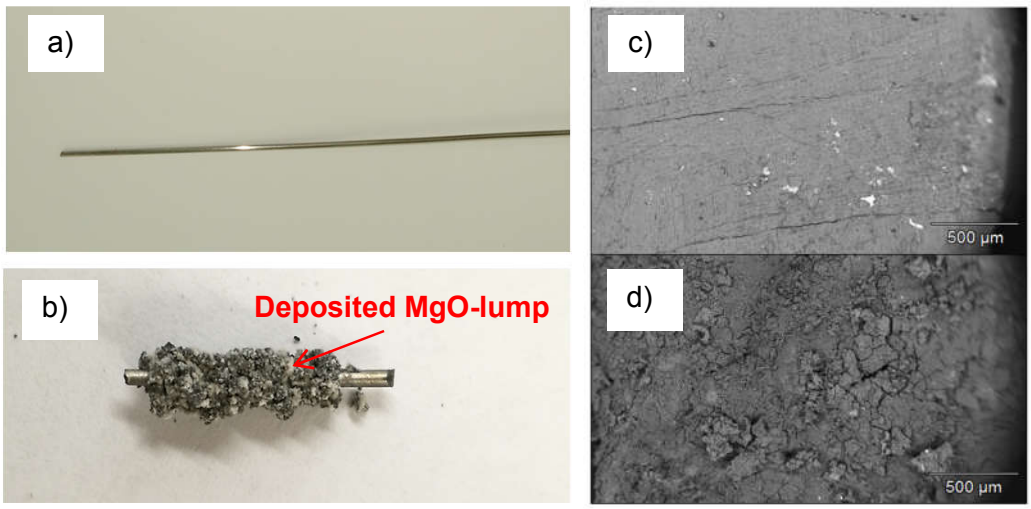

Figure 5: Before electrolysis, a) tungsten cathode, and c) scanning electron microscope (SEM) image of smooth Mg anode surface; After electrolysis, b) tungsten cathode with MgO deposits, and d) SEM image of rough Mg anode surface.

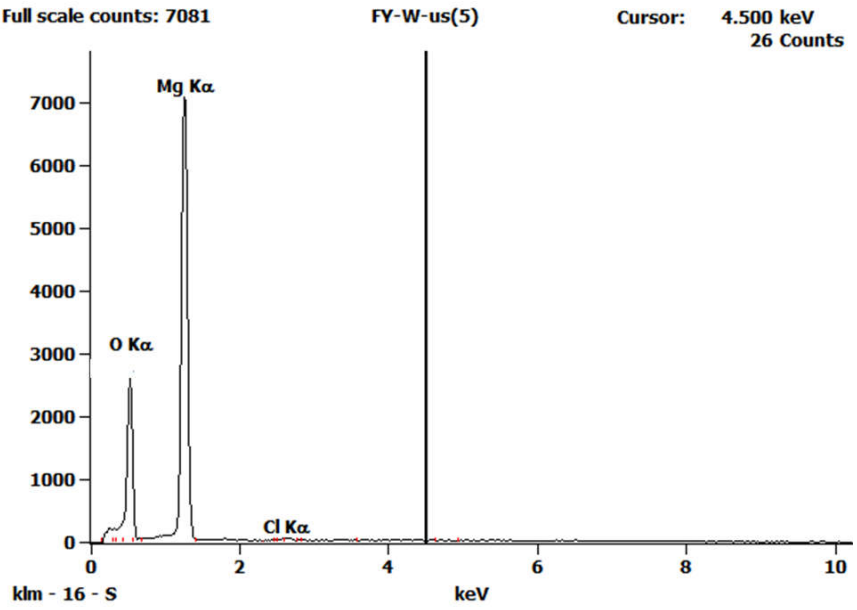

Figure 6: Energy-dispersive X-ray spectroscopy (EDS) on the lump shown in Figure 5b.

After 9 min of electrochemical purification at 500°C using the pulsed potential as shown in Figure 7 a), the peak current representing the reduction of $MgOH^+$ was reduced significantly to ~5 mA (see Figure 7 b) from ~70 mA (see Figure 3), i.e., the peak current density was reduced to ~31 mA/cm^2. This means that the concentration of $MgOH^+$ in the melt was reduced to ~1184±223 from ~16713±3325 ppm O in weight (only ~7% of that in unpurified melt) according to Eq. (12). Moreover, the scanning electron microscope (SEM) images on the surfaces of the Mg anode before and after electrolysis (Figure 5 c and d) show that the smooth surface of the Mg anode was changed due to the electrolysis. Moreover, the weight of the Mg anode was reduced significantly. These facts indicated that the Mg anode was consumed according to reaction (II) in section 2.3.2, when $MgOH^+$ in the melt was reduced at

the cathode. Figure 8 schematically shows the assumed reactions and observed phenomena on the W-cathode and Mg-anode in the electrochemical salt purification.

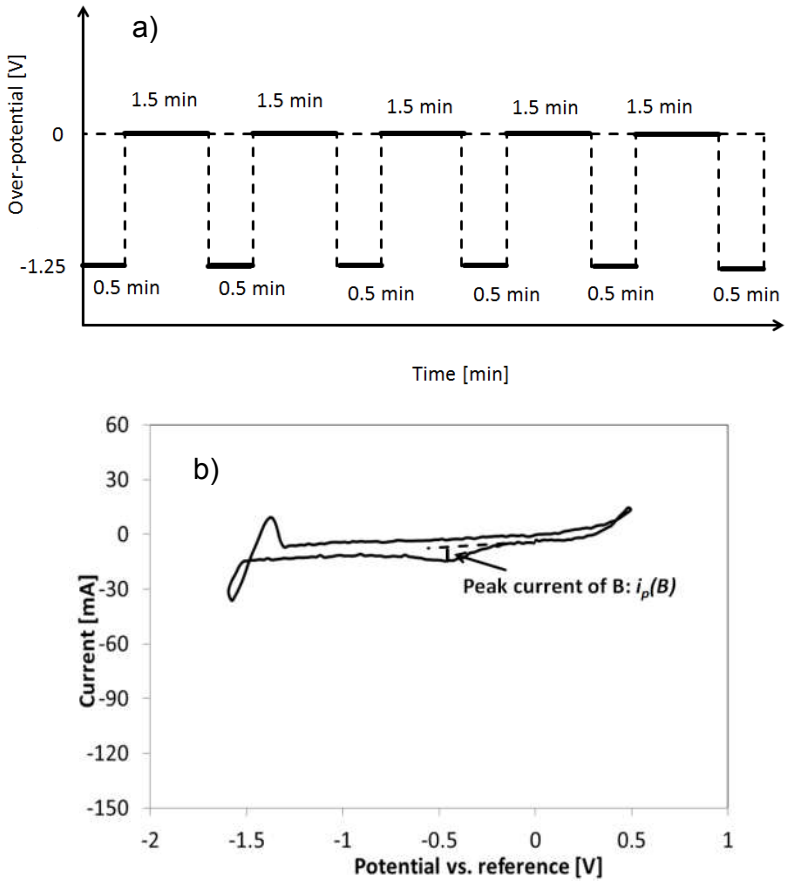

Figure 7: a) Pulsed over-potential applied during the electrochemical purification process, b) Cyclic voltammograms of molten $MgCl_2$/NaCl/KCl after purification at 500°C. Sweep rate: 200 mV/s. $i_p(B)$: peak current for reaction B. W quasi-reference electrode.

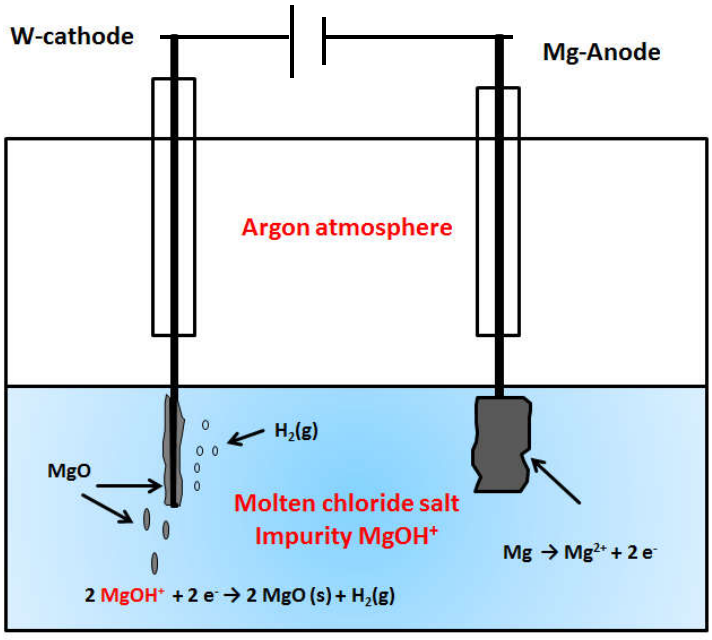

Figure 8: Schematic of assumed reactions and observed phenomena on the W-cathode and Mg-anode in the electrochemical purification using pulsed over-potential.

3.2. Effect of impurity in chloride salt on its corrosivity

As a comparison of the corrosivities of the unpurified and purified salts at high temperatures, the molten salt purified at 500°C was heated to 700°C (**Experiment 1**), while a salt sample with the same composition was heated to 700°C without salt purification (**Experiment 2**), as described in Section 2.2.

Figure 9 shows that the impurity $MgOH^+$ in the unpurified salt at 700°C (**Experiment 2**) had a concentration of ~1175±238 ppm O in weight (peak current of ~20 mA, peak current density of ~125 mA/cm^2), while the $MgOH^+$ concentration in the purified salt (**Experiment 1**) was reduced to only ~176±36 ppm O in weight (peak current of ~3 mA, peak current density of ~19 mA/cm^2) due to thermal decomposition of $MgOH^+Cl^-$ to MgO and HCl [19]. Both CV experiments were performed immediately when the salts were heated to 700°C.

Figure 10 shows the potentiodynamic polarization (PDP) curves of Incoloy 800 H in the unpurified and purified salts at 700°C. The PDP measurements were performed immediately after the CV experiments. The corrosion current I_{corr} of Incoloy 800 H in the unpurified salt obtained from the PDP curve via Tafel lines was ~1 mA (i.e., corrosion current density of ~131 μA/cm^2), which represented a corrosion rate of ~1550 μm/year according to Eq. (13). The corrosion current of Incoloy 800H in the purified salt was significantly reduced to ~200 μA (corrosion current density of ~26 μA/cm^2), i.e., the corrosion rate was reduced to ~310 μm/year, ~20% of that in the unpurified salt. Moreover, the corrosion potential of Incoloy 800 H in the purified salt (E_{corr} = -0.34 V vs. reference electrode) was much lower than that in unpurified salt (E_{corr} = -0.18 V vs. reference electrode). SEM and EDX cross-section images of the In 800 H alloy sample after Experiment 1 and 2 are shown in Figure 11 and Figure 12, respectively. The thickness of the corrosion layer is measured to be ~100 μm and ~230 μm in Experiment 1 and 2, respectively. Thus, the corrosion rate of the alloy sample in Experiment 1 and 2 is ~1.9 and ~6.7 mm/year, respectively. These results indicate that reducing the impurity by the electrolysis presented here could significantly reduce the corrosivity of the molten chloride salt.

Atomic absorption spectroscopy (AAS) was used to measure the concentrations of the alloying elements Cr, Fe and Ni dissolved in the chloride salts after Experiment 1 and 2. Figure 13 shows that in both salts no Ni was observed (AAS detection limit of 10 ppm in weight). This means that less Ni was dissolved from the alloy into the molten chloride salts due to lower reactivity compared to Cr and Fe [40] (see Table 3). Moreover, the concentration of Cr dissolved in the salt was much higher than that of Fe. This indicates that Cr was preferentially dissolved in the molten salt in these experiments. This agrees with the experimentally obtained electromotive force (EMF) series in $MgCl_2$-NaCl-KCl Eutectic molten salt at 475°C shown in Table 3 and the standard Gibbs free energy of the reaction between

MgOHCl and the alloying element Cr, Fe and Ni. Compared to Experiment 1, the concentration of Cr and Fe in the salt in Experiment 2 was much higher. This agrees with the results shown in Section 3.1 that the corrosion rate in the unpurified salt without immersion of Mg electrode (Experiment 2) was higher than that in the purified salt with immersion of Mg electrode (Experiment 1). The immersion of Mg electrode in the molten salt could keep the corrosive impurity in the purified salt at a low concentration, since during the experiment H_2O and O_2 in the sweep gas or from the air due to the leakage of the autoclave may have entered into the molten salt.

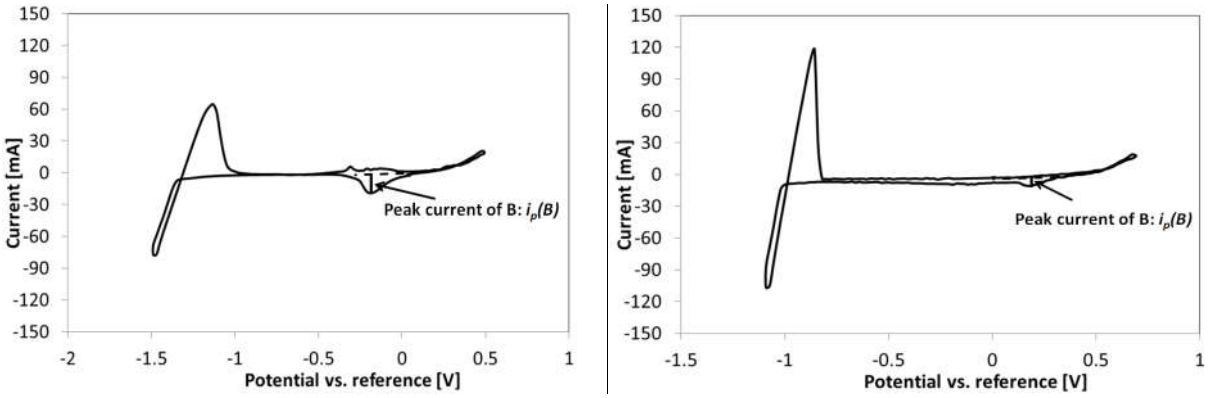

Figure 9: Cyclic voltammograms of molten $MgCl_2$/NaCl/KCl (60-20-20 mol%) at 700°C. Left: unpurified salt (Experiment 2); right: purified salt (Experiment 1). Potential sweep rate: 200 mV/s; Working electrode: tungsten, 0.16 cm^2 contact area with the melt. W quasi-reference electrode was used.

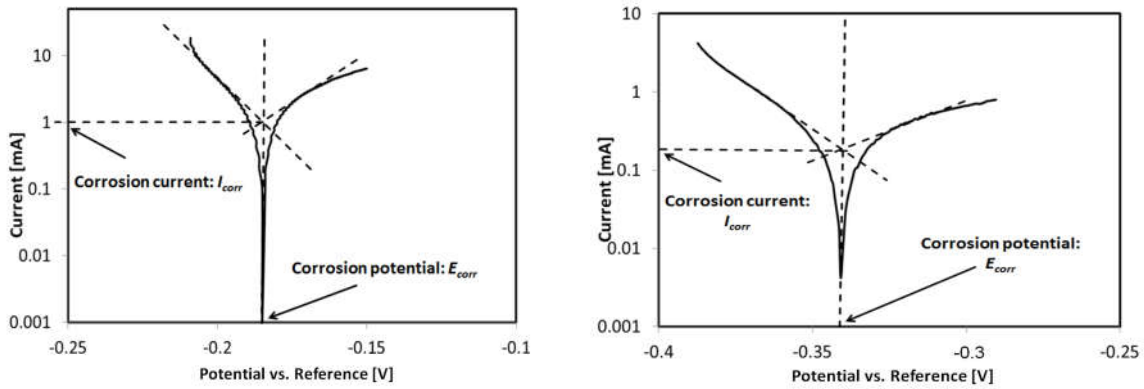

Figure 10: Potentiodynamic polarization curves of molten $MgCl_2$/NaCl/KCl (60-20-20 mol%) at 700°C. Left: not purified (corrosion current I_{corr}: ~1 mA, corrosion potential E_{corr}: -0.18 V vs. reference); right: purified electrochemically using bulk magnesium as the anode at 500°C (corrosion current I_{corr}: ~200 µA, corrosion potential E_{corr}: -0.34 V vs. reference). Potential sweep rate: 1 mV/s; Working electrode: Incoloy 800 H, ~7.6 cm^2 contact area with the melt; counter electrode: tungsten; W quasi-reference electrode was used.

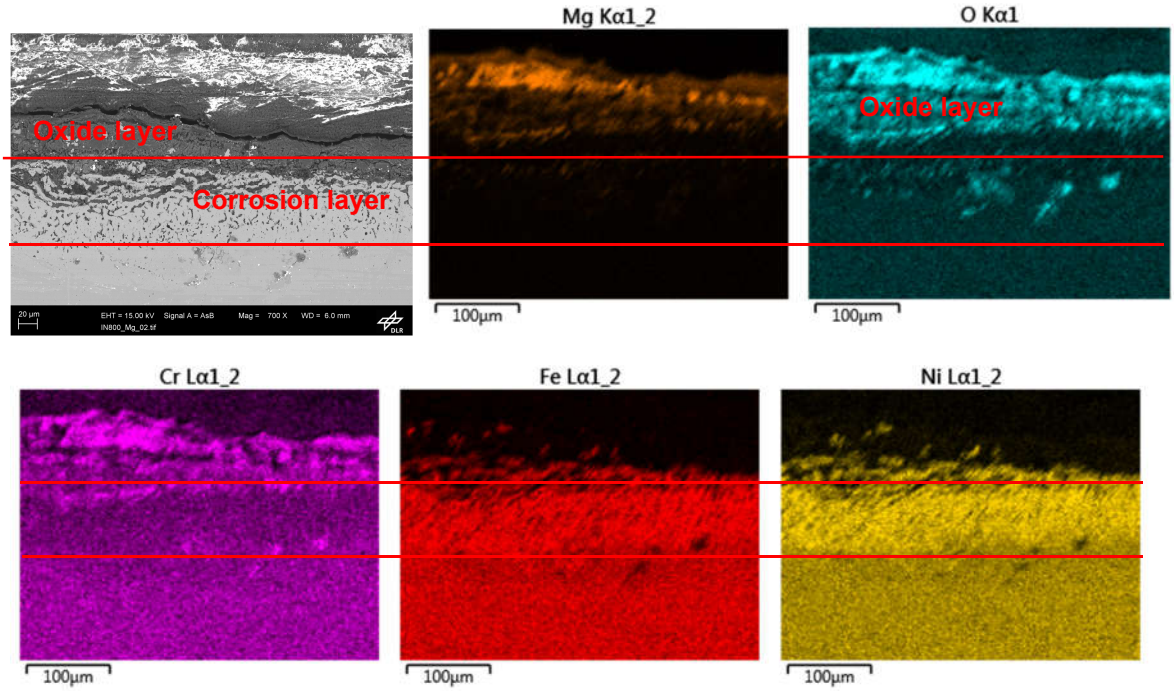

Figure 11: SEM and EDX cross-section images of In 800 H alloy sample after Experiment 1 in purified salt.

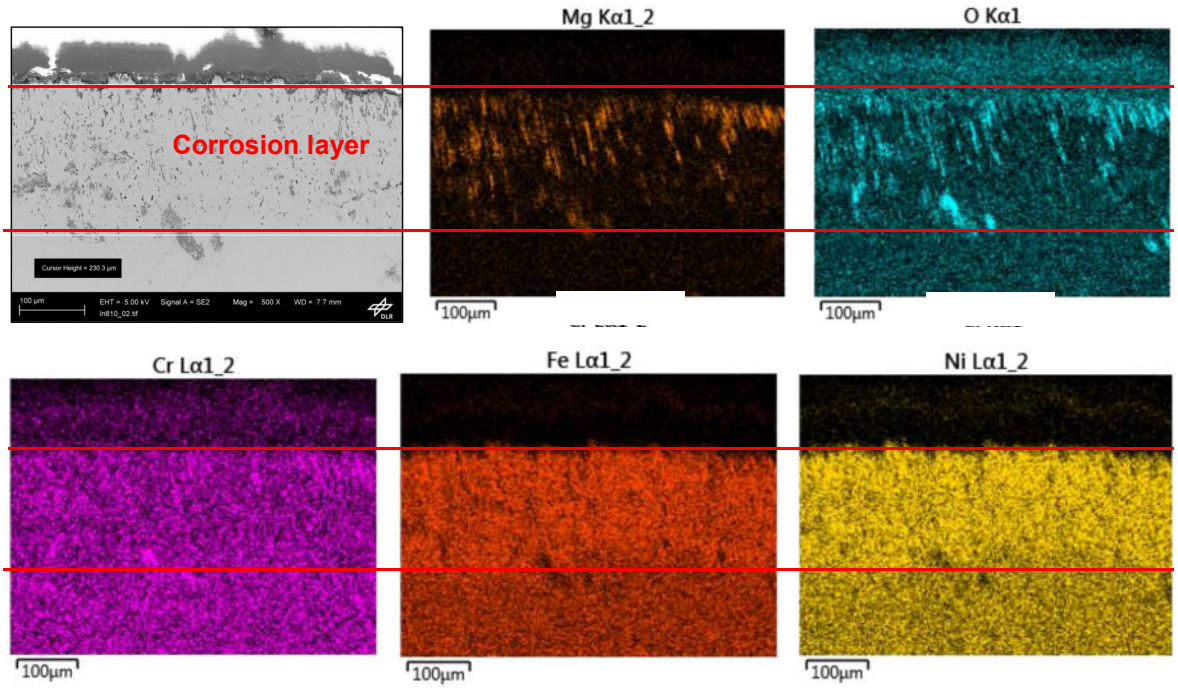

Figure 12: SEM and EDX cross-section images of In 800 H alloy sample after Experiment 2 in unpurified salt.

The concentrations of alloying elements (i.e., Cr and Fe) dissolved in the chloride salt after the corrosion experiments were used to estimate the equivalent corrosion depths of In 800 H in purified and unpurified salt. They are 291 and 1490 µm/year, respectively, which compare well with the CRs determined by PDP (~310 and ~1550 µm/year in purified and unpurified

salt, respectively). This confirms the effect of the electrochemical salt purification on reducing its corrosivity.

Table 3: Electromotive force (EMF) series in $MgCl_2$-NaCl-KCl eutectic molten salt at 475°C [40]

	Mg^{2+}/Mg	Cr^{2+}/Cr	Fe^{2+}/Fe	Ni^{2+}/Ni
EMF / V (vs. Pt^{2+}/Pt)	-2.646	-1.396	-1.183	-0.792

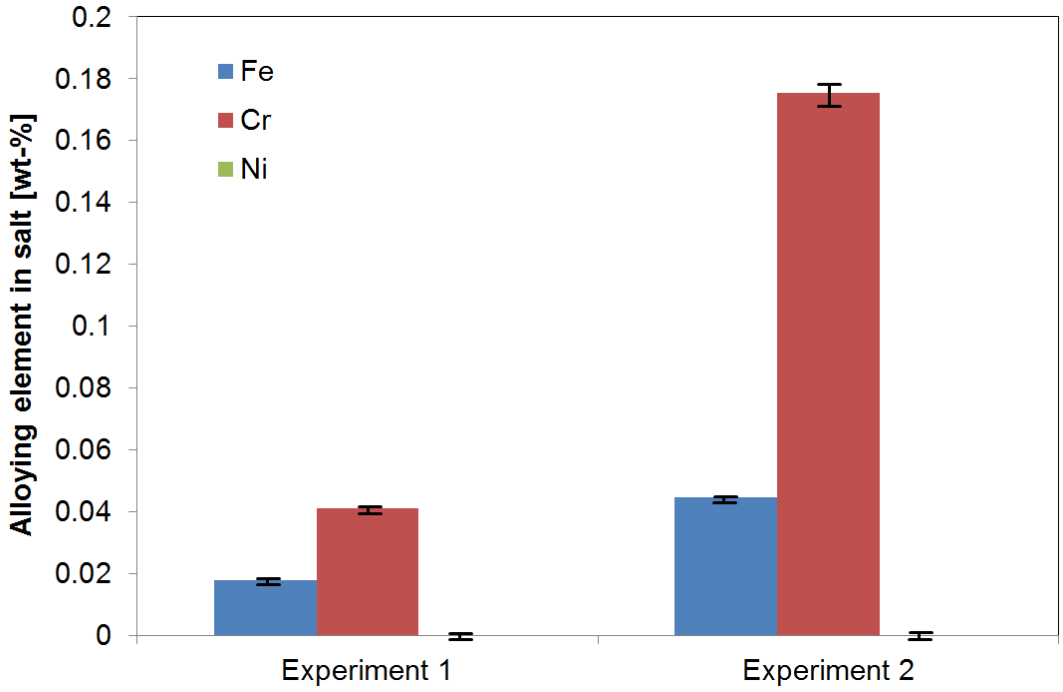

Figure 13: Alloying elements Cr, Fe and Ni dissolved in the chloride salts after 450 h (Experiment 1, purified salt) and 340 h (Experiment 2, unpurified salt) exposure, measured with AAS. Ni Content is below the detection limit of AAS (10 ppm in weight). The error bar represents the standard deviation of three measurements.

4. Conclusions

An electrolysis method with a Mg-anode has been investigated to purify the molten chloride salts, i.e., to reduce the concentration of the corrosive impurity $MgOH^+$, to reduce the corrosivity of the molten chloride salts at high temperatures.

The main conclusions of this work are:

- The corrosive impurity $MgOH^+$ can be significantly reduced by electrochemical salt purification using a Mg-anode at 500°C. Cyclic voltammetry measurements show that impurity concentration in purified salt is only ~7% of that in unpurified salt at 500°C.
- By reducing the corrosive impurity, the corrosion rate of Incoloy 800 H can be significantly reduced. The potential of the alloy moved to more negative values, i.e.,

the molten chloride salt is less oxidative. PDP results show that the corrosion rate of Incoloy 800 H in purified salt is only ~20% of that in unpurified salt at 700°C.

- The equivalent corrosion depths (ECDs) of In 800 H in purified and unpurified salt were estimated using the concentrations of Cr and Fe dissolved in the melt after the experiments, which were measured by AAS. The estimated ECDs compare well with the CRs determined by PDP. This confirms the effect of the electrochemical salt purification on reducing its corrosivity.

Acknowledgments

This research has been performed within the DLR-DAAD fellowship programme (grant number 57265854), which is funded by German Academic Exchange Service (DAAD) and German Aerospace Center (DLR). The authors would like to thank Fan Yang, a master student from Stuttgart University, their colleagues Dr. Carolina Villada, Markus Braun and Jochen Forstner at the DLR-Institute of Engineering Thermodynamics for their support. The work at the National Renewable Energy Laboratory (NREL) was financially supported by the U.S. Department of Energy under Contract No. DE-AC36-08-GO28308.

References

1. REN21, Renewables 2016: Global Status Report, 2016, ISBN 978-3-9818107-0-7.
2. M. Mehos, C. Turchi, J. Vidal, M. Wagner, Z. Ma, C. Ho, W. Kolb, C. Andraka, A. Kruizenga, Concentrating solar power Gen3 demonstration roadmap. National Renewable Energy Laboratory (NREL) Technical Report: NREL/TP-5500-67464, 2017.
3. G. Mohan, M. Venkataraman, J. Gomez-Vidal, J. Coventry, Assessment of a novel ternary eutectic chloride salt for next generation high-temperature sensible heat storage, Energy Convers. Manag. 167 (2018) 156-164.
4. X. Xu, X. Wang, P. Li, Y. Li, Q. Hao, B. Xiao, H. Elsentriecy, D. Gervasio, Experimental test of properties of KCl–$MgCl_2$ eutectic molten salt for heat transfer and thermal storage fluid in concentrated solar power systems. J. Sol. Energy Eng. 140(5) (2018) 051011 (9 pages).
5. Y. Li, X. Xu, X. Wang, P. Li, Q. Hao, B. Xiao, Survey and evaluation of equations for thermophysical properties of binary/ternary eutectic salts from NaCl, KCl, $MgCl_2$, $CaCl_2$, $ZnCl_2$ for heat transfer and thermal storage fluids in CSP, Sol. Energy 152 (2017) 57–79.
6. K. Vignarooba, P. Pugazhendhi, C. Tucker, D. Gervasio, A.M. Kannan, Corrosion resistance of Hastelloys in molten metal-chloride heat-transfer fluids for concentrating solar power applications, Sol. Energy 103 (2014) 62-69.

7. J. Gasia, L. Miró, L.F. Cabeza, Review on system and materials requirements for high temperature thermal energy storage. Part 1: General requirements, Renew Sust. Energ. Rev. 75 (2017) 1320-1338.
8. W. Ding, A. Bonk, T. Bauer, Corrosion behavior of metallic alloys in molten chloride salts for thermal energy storage in concentrated solar power plants - A review, Front. Chem. Sci. Eng. 12(3) (2018) 564–576.
9. T. Bauer, N. Pfleger, D. Laing, S. Kaesche, High-temperature Molten Salts for Solar Power Application. Chapter 20 in book: molten salts chemistry, p. 415, 2013, ISBN: 978-0-12-398538-5.
10. C. Villada, A. Bonk, T. Bauer, F. Bolívar, High-temperature stability of nitrate/nitrite molten salt mixtures under different atmospheres. Appl. Energy 226 (2018) 107-115.
11. A. Bonk, S. Sau, N. Uranga, M. Hernaiz, T. Bauer, Advanced heat transfer fluids for direct molten salt line-focusing CSP plants, Prog. Energy Combust. Sci. 67 (2018) 1339–51.
12. A.M. Kruizenga, Corrosion Mechanisms in Chloride and Carbonate Salts. SANDIA Report SAND2012-7594, 2012.
13. K. Vignarooban, X. Xu, A. Arvay, K. Hsu, A.M. Kannan, Heat transfer fluids for concentrating solar power systems – A review, Appl. Energy 146 (2015) 383-396.
14. Y. Tian, C.Y. Zhao, A review of solar collectors and thermal energy storage in solar thermal applications, Appl. Energy 104 (2013) 538-553.
15. K. Vignarooban, X. Xu, K. Wang, E.E. Molina, P. Li, D. Gervasio, A.M. Kannan, Vapor pressure and corrosivity of ternary metal-chloride molten-salt based heat transfer fluids for use in concentrating solar power systems, Appl. Energy 159 (2015) 206-213.
16. G.Y. Lai, High-Temperature Corrosion and Materials Applications, Chapter 15 in book: Molten Salt Corrosion, ASM International, 2007.
17. S. Guo, J. Zhang, W. Wu, W. Zhou, Corrosion in the molten fluoride and chloride salts and materials development for nuclear applications, Prog. Mater. Sci. 97 (2018) 448-487.
18. H.R. Copson, Corrosion of heating electrodes in molten chloride baths, J. Electrochem. Soc. 100(6) (1953) 257-264.
19. G.J. Kipouros, D.R. Sadoway, A thermochemical analysis of the production of anhydrous $MgCl_2$, J. Light Met. 1(2) (2001) 111–117.
20. L. Maksoud, T. Bauer, Experimental investigation of chloride molten salts for thermal energy storage applications. 10th International Conference on Molten Salt Chemistry and Technology, 10.-12. June 2015, Shenyang, China.
21. D.F. Williams, Assessment of candidate molten salt coolants for the NGNP/NHI heat-transfer loop. Oak Ridge National Laboratory, 2006.

22. W. Ding, H. Shi, Y. Xiu, A. Bonk, A. Weisenburger, A. Jianu, T. Bauer, Hot corrosion behavior of commercial alloys in thermal energy storage material of molten $MgCl_2$/KCl/NaCl under inert atmosphere, Sol. Energy Mater. Sol. Cells 184 (2018) 22-30.
23. B. Liu, X. Wei, W. Wang, J. Lu, J. Ding, Corrosion behavior of Ni-based alloys in molten NaCl-$CaCl_2$-$MgCl_2$ eutectic salt for concentrating solar power, Sol. Energy Mater. Sol. Cells 170 (2017) 77–86.
24. V.L. Cherginets, T.P. Rebrova, Studies of some acid-base equilibria in the molten eutectic mixture KCl-LiCl at 700°C, Electrochim. Acta 45(3) (1999) 469-476.
25. D.L. Maricle, D.N. Hume, A new method for preparing hydroxide-free alkali chloride melts, J. Electrochem. Soc. 107(4) (1960) 354-356.
26. J. Ambrosek, Doctoral thesis: Molten Chloride Salts for Heat Transfer in Nuclear Systems, in Nuclear Engineering and Engineering Physics, University of Wisconsin-Madison, 2011.
27. B.L. Garcia-Diaz, L. Olson, M. Martinez-Rodriguez, R. Fuentes, H. Colon-Mercado, J. Gray, High temperature electrochemical engineering and clean energy systems, J. South Carol. Acad. Sci. 14(1) (2016) Article 4.
28. B. Mishra, D.L. Olson, Corrosion of refractory alloys in molten lithium and lithium chloride, Min. Proc. Ext. Met. Rev. 22(4-6 SCPEC. ISS) (2001) 369-388.
29. J.E. Indacochea, J.L. Smith, K.R. Litko, E.J. Karell, A.G. Rarez, High-temperature oxidation and corrosion of structural materials in molten chlorides, Oxid. Met. 55(1-2) (2001) 1-16.
30. J.E. Indacochea, J.L. Smith, K.R. Litko, E.J. Karell, Corrosion performance of ferrous and refractory metals in molten salts under reducing conditions, J. Mater. Res. 14(5) (1999) 1990-1995.
31. W. Ding[*,1], H. Shi[*,1], A. Jianu, Y. Xiu, A. Bonk, A. Weisenburger, T. Bauer, Molten chloride salts for high-temperature thermal energy storage: Mitigation strategies against corrosion of structural materials, Sol. Energy Mater. Sol. Cells 193 (2019) 298-313.
32. W. Ding, A. Bonk, J. Gussone, T. Bauer, Cyclic voltammetry for monitoring corrosive impurities in molten chlorides for thermal energy storage, Energy Procedia 135 (2017) 82-91.
33. W. Ding, A. Bonk, J. Gussone, T. Bauer, Electrochemical measurement of corrosive impurities in molten chlorides for thermal energy storage, J. Energ. Storage 15 (2018) 408–414.
34. J. Gomez-Vidal, R. Tirawat, Corrosion of alloys in a chloride molten salt (NaCl-LiCl) for solar thermal technologies, Sol. Energy Mater. Sol. Cells 157 (2016) 234-244.
35. J.W. Wang, C.Z. Zhang, Z.H. Li, H.X. Zhou, J.X. He, J.C. Yu, Corrosion behavior of nickel-based superalloys in thermal storage medium of molten eutectic NaCl-$MgCl_2$ in atmosphere, Sol. Energy Mater. Sol. Cells 164 (2017) 146–155.

36. R.A. Skar, Doctoral thesis: Chemical and electrochemical characterisation of oxide/hydroxide impurities in the electrolyte for magnesium production. Norwegian University of Science and Technology (NTNU), 2001.
37. U.S. Patent Application 16/003,229 "Methods for reducing the corrosiveness of a fluid material for a high-temperature range and devices therefore" filed on June 8th, 2018. Authors: J. Vidal (NREL), W. Ding and T. Bauer (German DLR). NREL control: PROV/18-58.
38. A. Komura, H. Imanaga, N. Watanab, K. Nakanishi, Solubility of magnesium in molten magnesium chloride, J. Soc. Chem. Ind. Japan 71(12) (1968) 1976-1979 (in Japanese).
39. B. Welz, M. Sperling, Atomic absorption spectrometry. 3rd Edition, 2008, ISBN: 978-3-527-61168-3.
40. J.A. Plambeck, Electromotive force series in molten salts, J. Chem. & Eng. Data 12(1) (1967) 77-82.